



Radiation and cloud-base lowering fog events: Observational analysis and evaluation of WRF and HARMONIE



Carlos Román-Cascón^{a,b,*}, Carlos Yagüe^a, Gert-Jan Steeneveld^c, Gema Morales^d, Jon A. Arrillaga^a, Mariano Sastre^a, Gregorio Maqueda^a

^a Dept. Física de la Tierra y Astrofísica, Universidad Complutense de Madrid, Spain

^b Laboratoire d'Aérodynamique, University of Toulouse, CNRS, France

^c Meteorology and Air quality Section, Wageningen University, the Netherlands

^d Agencia Estatal de Meteorología (AEMET), Madrid, Spain

ARTICLE INFO

Keywords:

Fog
Radiation
Cloud-base-lowering
WRF
HARMONIE
Model skill

ABSTRACT

Most of the effects caused by fog are negative for humans. Yet, numerical weather prediction (NWP) models still have problems to simulate fog properly, especially in operational forecasts. In the case of radiation fog, this is partially caused by the large sensitivity to many aspects, such as the synoptic and local conditions, the near-surface turbulence, the aerosol and droplet microphysics, or the surface characteristics, among others. This work focuses on an interesting 8-day period with several alternating radiation and cloud-base lowering (CBL) fog events observed at the Research Centre for the Lower Atmosphere (CIBA) in the Spanish Northern Plateau. On the one hand, radiation fog events are associated with strong surface cooling leading to high stability close to the surface and low values of turbulence, giving rise to shallow fog. The evolution of this type of fog is markedly sensitive to the dynamical conditions close to the surface (i.e., wind speed and turbulence). On the other hand, CBL fog presents deeper thickness associated with higher values of turbulence and less stability. Subsequently, we evaluated the fog-forecasting skill of two mesoscale models (WRF and HARMONIE) configured as similar as possible. Both models present more difficulties simulating radiation fog events than CBL ones. However, the duration and vertical extension of the CBL fog events is normally overestimated. This extended-fog avoids the surface radiative cooling needed to simulate radiation fog events formed the following nights. Therefore, these periods with alternating CBL and radiation fog are especially challenging for NWP models.

1. Introduction

Fog affects human life in many forms. Only a few impacts are positive, like the extra water supply in freshwater-poor regions using fog collectors (Shanyengana et al., 2002; Roco et al., 2018) or the moisture (and nutrients) source for some plants (Azevedo and Morgan, 1974; Dawson, 1998). However, all the other fog effects are negative and undesired by humans. The terrestrial, aerial and maritime transportation is difficult and often dangerous under foggy conditions due to the associated reduction in visibility (Fabbian et al., 2007; Fu et al., 2010; Bartok et al., 2012). Thus, the economic costs of fog (accidents, flights cancellations, etc.) are estimated to be similar than those associated with the destruction caused by tornadoes (Gultepe et al., 2007). Moreover, the combination of pollution and fog causes severe and significant problems for human health in some areas, increasing, for example, the hospital visits for asthma episodes (Tanaka et al., 1998).

Even having all these negative influences on humans, the prediction of fog is still a main challenge for the meteorological services (Zhou et al., 2012; McCabe et al., 2016) since numerical weather prediction (NWP) models still have problems simulating this phenomenon (Steenefeld et al., 2015). These fog-forecasting difficulties are affected by different aspects. The first issue is related to the own complexity of fog, which forms as result of a delicate combination of appropriate surface dynamics and turbulence (e.g., Zhou and Ferrier, 2008), radiation (e.g., Funk, 1962), aerosols and droplets chemistry and microphysics (e.g., Mohan and Payra, 2009), large-scale synoptic conditions (e.g., Hyvärinen et al., 2007) and/or specific interactions with the local features, such as topography (e.g., Hang et al., 2016). In many cases, global models have scales that are not appropriate to reproduce fog, and the use of mesoscale ones is encouraged (Teixeira, 1999). Thus, mesoscale NWP models need to simulate correctly all these physical processes to perform successful simulations of fog. However, the fog

* Corresponding author at: Dept. Física de la Tierra y Astrofísica, Universidad Complutense de Madrid, Spain
E-mail address: carlosromancascon@ucm.es (C. Román-Cascón).

forecasting can be also affected by issues related to the model itself: possible errors in initial and boundary conditions (e.g., Bergot and Guedalia, 1994; Hu et al., 2014), appropriate spin-up times (e.g., Román-Cascón et al., 2016a), limitations in the vertical/horizontal resolution (e.g., Philip et al., 2016; Boutle et al., 2016) or inappropriate parameterizations of sub-grid scale processes (e.g., Román-Cascón et al., 2012; Chaouch et al., 2017). These are some of the reasons why in other cases, the use of 1D models and statistical downscaling techniques are also used, especially in predictions needed at specific points, e.g., in airports (Cornejo-Bueno et al., 2017). Since fog can form over land or sea following different processes, the ability of the model simulating fog will also differ depending on the fog type.

On the one hand, the most common (and probably studied) fog type is radiation fog, formed as a result of the surface radiative cooling during the night (Bergot et al., 2007; Gultepe et al., 2007). Many observational and/or modelling studies have focused on this type of fog (e.g., Terradellas et al., 2008; Van der Velde et al., 2010; Bergot, 2013; Price et al., 2018, among many others), but models still have problems simulating it, especially when its formation is not imposed by the local topography (Müller et al., 2010). The characteristics of radiation fogs are variable, from short-lived, not-mixed and shallow fog events of a few meters to persistent, well-mixed and deep events of several hundreds of meters (Duynkerke, 1999; Román-Cascón et al., 2016b). Radiation fog can start its dissipation from the lower layers close to the surface or from the upper ones following different mechanisms, which are normally associated with increases in temperature, wind or turbulence. Several radiation fog events are often dissipated or elevated from the surface after sunrise when the daytime convection starts. This process can lead to clear skies after some minutes/hours, but in some cases the fog is transformed into low stratus clouds that can persist in the area even during the whole daytime.

On the other hand, the so-called cloud-base lowering (CBL) fog forms as the result of the lowering of the base of low-stratus clouds. CBL fog events are common in many areas of the world (Goodman, 1977; Tardif and Rasmussen, 2007; Van Schalkwyk and Dyson, 2013) and have been exhaustively studied in coastal and offshore areas (e.g., Oliver et al., 1978; Bari et al., 2015). However, they are also formed over land (Duynkerke and Hignett, 1993; Koračín et al., 2001; Roco et al., 2018), where they have been less studied. In some cases, CBL fog is observed after the descending of low-stratus clouds that were

previously fog (process commented in the previous paragraph). Thus, these periods are characterized by: (1) radiation fog; (2) low-stratus clouds formed by fog dissipation at the surface or fog elevation and; (3) CBL fog formed by the descending of low stratus. Unlike radiation fog, CBL fog does not require a net radiative cooling at the surface for its formation; in fact, the own existence of the stratus cloud can dampen this cooling. These periods with alternating radiation-CBL fog are common in many areas; however, literature is scarce on their observational analysis (e.g., Dupont et al., 2012, 2018), as well as in the evaluation of their simulation by models considering their specific fog formation processes.

This lack of research is the main motivation of this study. The first objective of this work aims to better understand the conditions in which CBL and radiation fog events form through an exhaustive observational analysis of their features. In this sense, we have analysed a particular period of 8 days characterized by alternating CBL and radiation fog at the Research Centre for the Lower Atmosphere (CIBA) site in the Spanish Northern Plateau during January 2016. The instrumentation specifically deployed for investigating the development of fog in the site allows this study. On the other hand, it results especially interesting to evaluate state-of-the-art mesoscale models simulating these fog events of different characteristics, as well as to quantify their skill simulating the key near-surface meteorological variables controlling the fog evolution. For this aim, we analyse how this period is simulated by the Weather Research and Forecasting (WRF) model and the HIRLAM ALADIN Research on Mesoscale Operational NWP In Euromed (HARMONIE) model set with the AROME configuration and with similar configuration than WRF. Hence, the second objective of this work is focused on detecting the strengths and weaknesses of these models under different fog-type specific conditions. These findings are expected to be valuable to improve the operational forecasting of fog, as well as the model development.

This work is organised as follows: Section 2 presents the observational data used to characterize the events at the site, the configuration of the models and an introduction to the analysed period. Section 3 presents an exhaustive observational description and analysis of the model skill for each fog event. Section 4 gathers an overview of the model skill for all the events, discussing the results obtained for CBL and radiation fog. Finally, the main findings are summarised in Section 5.

Table 1
Observational measurements used, height(s) and type of sensor.

Variable	Height (m)	Instrument
Visibility	2, 30, 70, 100	Biral SWS 100
Temperature	1.5, 5, 10, 50, 85	Theodor Friedrichs 3032.02
Specific humidity	1.5	Theodor Friedrichs 3032.02
Wind speed	10	Theodor Friedrichs 4035.01
Turbulent kinetic energy (TKE)	10	Sonic anemometer METEK-USA-1

Table 2
Information about models configuration.

	WRF-ARW	HARMONIE-AROME
Horizontal resolution	2.5 km	2.5 km
Model domain	300 × 300 points	300 × 300 points
Initial and boundary conditions	ECMWF operational analysis	ECMWF operational analysis
PBL scheme	TKE-I scheme MYNN	TKE-I CBR
LSM	Noah	SURFEX
Microphysics	WDM6	ICE3
Number of vertical levels	61	65
Time step	60 s	60 s
Leading time	24 h	24 h

Table 3

Main characteristics from the observational analysis of fog events. The represented values for the different variables (2-m temperature, 2-m specific humidity, 10-m wind speed, turbulent kinetic energy, temperature difference between the levels of 10 and 2 m agl ($T_{10} - T_2$) and fog thickness) correspond to the mean calculated from the fog onset to its dissipation. Times are in UTC. The two last lines indicate the mean values for all the fog events of each type.

Event	Fog type	Onset time	Dissipation time	Duration (h)	T_2 (°C)	q_2 (g kg ⁻¹)	WS_{10} (m s ⁻¹)	TKE (m ² s ⁻²)	$T_{10} - T_2$ (°C)	Thickness (m)
1	Rad	Day 20 00:41	Day 20 04:23	3.7 (short)	-0.84	3.76	1.34	0.05	0.63	34
2	CBL	Day 20 23:09	Day 21 01:09	2.0 (short)	5.32	5.91	1.73	0.14	0.24	> 100
3	CBL	Day 21 18:32	Day 23 10:47	40.2 (persistent)	8.76	7.54	1.32	0.07	0.50	Variable
4	Rad	Day 23 19:29	Day 24 08:24	12.9 (long)	5.93	6.18	1.80	0.04	0.98	40
5	Rad	Day 26 02:53	Day 26 09:34	6.7 (intermediate)	2.51	4.83	1.17	0.03	1.81	27
6	CBL	Day 26 21:21	Day 27 10:16	13 (long)	3.90	5.38	1.52	0.11	0.20	Variable
RAD	//	//	//	7.8	2.53	4.92	1.44	0.04	1.14	33
CBL	//	//	//	18.4	5.99	6.27	1.52	0.11	0.31	Variable/ > 100

2. Observational data, models and period

2.1. Observational data

The observational data analysed and used for the model evaluation in this study have been collected at CIBA site during the period comprising from 19 to 27 January 2016. This site (41°48.92'N; 4°55.92'W, 840 m above sea level) is located over *Los Montes Torozos*, an elevated and extended plateau of 800 km² situated over the large and wide Spanish Northern Plateau. A more complete description of this site is provided in Cuxart et al. (2000), while the fog climatology of the site was studied in Román-Cascón et al. (2016a). This work showed how most of the radiation-fog events at CIBA are formed between November and February. The site is prone to the formation of radiation fog, in many cases alternated with low-stratus clouds and CBL fog, affecting considerably to the nearby airport of Valladolid (Guijo-Rubio et al., 2018). Table 1 shows information about the instruments measuring the different variables. Note how in this study we analyse, among other

variables, the observed fog thickness calculated using data from visibilimeters installed at 2, 30, 70 and 100 m. Hence, its uncertainty is determined by the distance between visibilimeters. For example, if the fog is observed at 30 m but not a 70 m, it indicates a fog thickness between 30 and 70 m. When the fog is observed at the four levels, we can only determine that the minimum fog thickness was 100 m.

2.2. Models

Two mesoscale models have been used to simulate this period: the WRF-ARW (Weather Research and Forecasting Advanced Research WRF) model (version 3.7.1) (Skamarock et al., 2005) and the non-hydrostatic convection-permitting HARMONIE (HIRLAM ALADIN Research on Mesoscale Operational NWP In Euromed) model version 40h1.1 set with the AROME configuration (Bengtsson et al., 2017). Both models were configured as similar as possible: one domain of 300 × 300 grid points with 2.5 km of grid spacing and approximately the same vertical levels positioned at similar heights (both models with

Table 4

Mean WRF and HARMONIE (HAR) model bias for different variables analysed for each fog event (strictly the fog period defined in Table 3).

	Event 1	Event 2	Event 3	Event 4	Event 5	Event 6	All (abs)
	Rad	CBL	CBL	Rad	Rad	CBL	
Fog							
WRF	No	Yes	Yes	No	Yes	Yes	4/6
HAR	No	Yes ^a	Yes	Yes ^a	Yes	No	4/6
Onset (h)							
WRF bias	//	-8	-1	//	-1	-6	-4 (4)
HAR bias	//	-5	+4	+3	+1	//	+0.75 (3.25)
Dissipation (h)							
WRF bias	//	+2	+1	//	+3	+1	+1.75 (1.75)
HAR bias	//	+10	+4	+4	+3	//	+5.25 (5.25)
T_2 (°C)							
WRF bias	-0.16	-2.20	-0.76	+0.58	+3.35	-0.67	+0.02 (1.28)
HAR bias	+1.84	-3.18	-1.26	+2.04	+2.06	+1.41	+0.49 (1.97)
q_2 (g kg ⁻¹)							
WRF bias	+0.09	-0.76	-0.33	+0.09	+1.35	-0.26	+0.03 (0.48)
HAR bias	+0.63	-1.09	-0.59	+0.95	+0.85	+0.40	+0.19 (0.75)
WS_{10} (m s ⁻¹)							
WRF bias	+0.16	-0.04	+0.50	+0.79	-0.23	-0.18	+0.17 (0.32)
HAR bias	+1.76	-0.74	+1.29	+1.05	+0.85	+0.66	+0.81 (1.06)
TKE (m ² s ⁻²)							
WRF bias	-0.01	-0.16	+0.03	+0.00	+0.09	+0.03	+0.00 (0.05)
HAR bias	+0.09	-0.28	+0.02	+0.09	+0.04	-0.07	-0.02 (0.10)

The mean bias for all the events is included in the last column, as well as the mean of event-biases in absolute values (in parenthesis).

^a Indicates that the fog was simulated following an incorrect formation mechanism.

4 levels below 100 m and 7 below 200 m). Although the HARMONIE-AROME model does not permit to be fully customizable, some changes have been done for the comparison: a smaller domain than the operational model, no assimilation, boundary conditions applied every 3 h and a model start not connected to previous forecasts. The WRF-ARW model has been configured with similar settings than HARMONIE-AROME (see Table 2).

A set of 7 simulations were performed, starting at 1200 UTC of each day from 18 to 25 January 2016 and running for 48 h. In order to evaluate the ability of the models forecasting radiation fog with certain lead time, we analyse only the simulation period from +24 h to +48 h, i.e., the second forecasted day. In fact, a previous study noted a better skill for the WRF model for the second forecasted day than the first one, probably due to spin-up issues (Román-Cascón et al., 2016a). Subsequently, a simulation composite was made with the 7 simulated days. Therefore, some discontinuities in the composite could be expected at 1200 UTC of each day, but in fact, these discontinuities are not clearly observed, which is a good indicator of the consistency between the runs performed on consecutive days.

A great part of the analyses shown hereinafter compares observed and simulated visibility. While direct visibility data are provided by the BIRAL SWS-100 visibilimeters, the visibility in the models have been calculated from liquid water content (LWC) output at the model levels. Since no information about the droplet spectra was available from the models, the LWC-visibility relationship given in Kunkel (1984) (eqs. 4 and 11) was used.

2.3. Analysed period

The synoptic situation over the Iberian peninsula during the period from 19 to 27 January 2016 was especially appropriate for the formation of radiation fog in predisposed areas over the Spanish Northern Plateau. A weak surface-pressure gradient existed during most part of the period, with a high pressure system first over central Europe and then extending towards the south. At 500 hPa, a relatively warm air mass existed during the whole period, except for days 20, 26 and 27 (Supplementary Fig. 1). This situation led to weak winds (Supplementary Fig. 3c) and to nocturnal surface cooling (Supplementary Fig. 3a) which caused the formation of several fog events over the area. An overview of the visibility during the whole period is shown in Supplementary Fig. 2a (note that each event will be shown with more detail in the results section). Six different events have been identified from the dark-grey colours in this figure, which represents horizontal visibility lower than 1 km obtained from the four visibilimeters installed at the site (Table 1), i.e., fog is detected when grey colour is observed at the lowest level (2 m). The fog events were separated into individual cases when the visibility at 2 m above ground level (agl) was higher than 1 km during at least 6 h between two consecutive events. From this detection, three events (event 1, 4 and 5) have been classified as radiation fog, formed as the result of the radiative cooling at the surface. The other three events (2, 3 and 6) showed the typical behaviour of cloud-base lowering (CBL) fog, resulting from the descending of low-cloud base. All the events have been simulated with the WRF and HARMONIE models (Supplementary Fig. 2b and c respectively), set with similar configurations (Table 2). The observed features are different for each fog event (main characteristics of the six fog events are shown in Table 3), as occurs for the model skill simulating fog. The model biases (differences between model and observed values) of the six fog events are summarised in Table 4. These differences among the events motivate an exhaustive individual analysis for each event rather than a global analysis and

evaluation, which could lead to wrong or inappropriate conclusions. Below, we show this case-by-case analysis, firstly with an observational description of each fog event and the associated surface variables and secondly with the analysis of the model skill for each specific event.

3. Observational analysis and model skill

3.1. Event 1: radiation fog (20 Jan 00:40–20 Jan 04:23 UTC)

3.1.1. Observational description

This fog event (Fig. 1a) is a short (3.7 h) and shallow (mean thickness of 34 m) pure radiation fog (Table 3) formed due to the surface radiative cooling during the afternoon preceding its formation. Mist

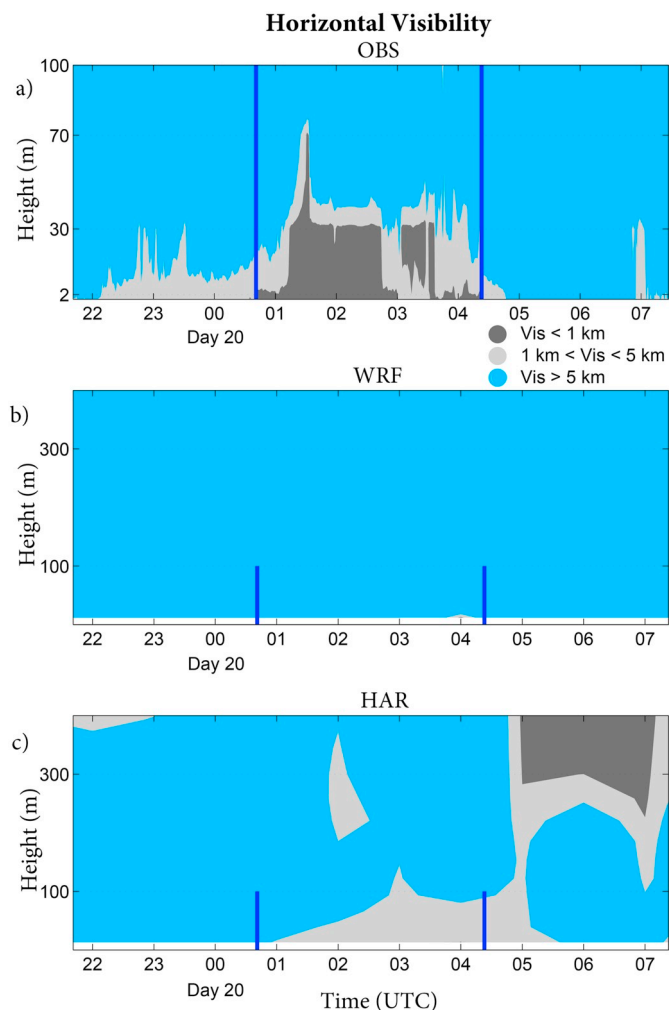


Fig. 1. (a) Fog observed at the CIBA site during event 1, from 20/01 at 0041 UTC to 20/01 at 0423 UTC. Fog is indicated with dark grey colours (vis < 1 km), mist with light grey colours (1 km < vis < 5 km) and visibility > 5 km with blue. Horizontal dotted lines indicate the heights with visibilimeters (2, 30, 70 and 100 m). Plotted data between these data are interpolated linearly. Vertical blue lines indicate the initial and end of the fog event. (b) Corresponding simulation by the WRF model up to 400 m. Blue vertical lines indicate the foggy period from figure a, only up to 100 m because of the lack of observational data above. (c) Idem for HARMONIE model. (For interpretation of the references to colour in this figure legend, the reader is referred to the web version of this article.)

(visibility between 1 and 5 km) was observed at 2 m around 2200 UTC before the fog formation (Fig. 1a). The fog was formed from the surface at 0040 UTC, growing up to > 30 m (and < 70 m) in a few minutes. Eventually, the fog grew up to the 70-m level for a short period around 0120 UTC but it remained with 30–70-m depth during the majority of the event. The fog dissipation started from above a few minutes before the surface dissipation at 0300 UTC. Subsequently, the visibility remained low at the surface (mist, < 5 km) but lower than 1 km at the 30-m level, i.e., the fog was transformed into very-low and shallow clouds close to the surface. Then, these very-low clouds descended to the surface level (2 m) again for almost 1 h, until the final fog dissipation at 0415 UTC approximately, well before sunrise. The fog did not re-appear during the following daytime.

Fig. 2 shows the associated surface variables during this event. The 2-m temperature (T_2) remained below 0 °C (mean of -0.84 °C) during the whole fog event, with a surface-based temperature inversion that

persisted during the event (see temperature at different levels in Fig. 2a), i.e. no effective mixing was observed in the lowest layers (the mean temperature difference between 10 and 2 m was 0.63 °C, see Table 3). These conditions were associated with relatively low values of the 10-m wind (WS_{10}) and turbulent kinetic energy (TKE) (Fig. 2b and d), with a mean WS_{10} of 1.34 m s $^{-1}$ and mean TKE of 0.05 m 2 s $^{-2}$ (Table 3) during the fog event. WS_{10} and TKE only increased between 0100 and 0200 UTC, when the fog eventually evolved to 70 m agl. A similar but more intense increase in wind speed and turbulence started at 0430 UTC, just after the final fog dissipation. q_2 ranged between 4 g kg $^{-1}$ before the event and 3.76 g kg $^{-1}$ during the fog due to the water vapour transformation into liquid water (Fig. 2c), highly influenced by T_2 . Note how the pre-fog/fog q_2 difference was quite small in this event compared to the other events. That is, the fog was formed after the condensation of a small amount of water vapour.

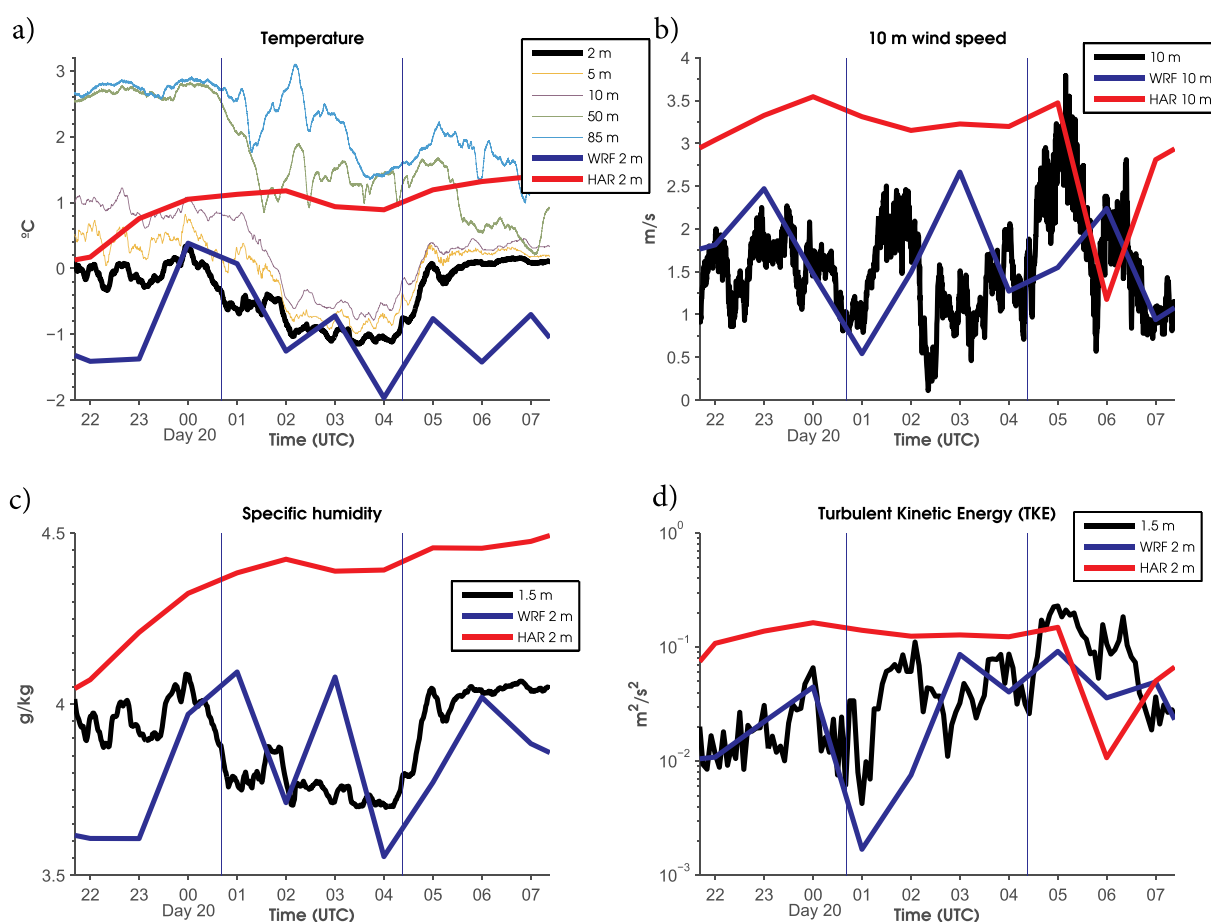


Fig. 2. Fog event 1. (a) Observed (thick black line) and simulated temperature (°C) at 2 m (WRF, blue line; HARMONIE, red line). Observed temperatures at 5 m (yellow), 10 m (purple), 50 m (green) and 85 m (light blue) are included in order to show surface-based temperature inversions and temperature convergence. (b) Idem for 10-m wind speed (m s $^{-1}$). (c) Idem for 1.5-m specific humidity (g kg $^{-1}$) (2 m for the models). (d) Idem for 1.5-m TKE (m 2 s $^{-2}$) (2 m for the models). Vertical blue lines indicate strictly the fog period. (For interpretation of the references to colour in this figure legend, the reader is referred to the web version of this article.)

3.1.2. Model skill

WRF is not able to simulate the fog at all (Fig. 1b). However, the simulated surface variables (blue thick lines in Fig. 2) present relatively low biases (see Table 4 for mean biases). We think that the reasons for the lack of fog simulation could be related to some microphysics limitations under freezing conditions or due to the insufficient number of vertical layers close to the surface for this very shallow event. A similar limitation for fog forecasting under freezing conditions has also been observed in previous works using the WRF model (Van der Velde et al., 2010).

HARMONIE is not able to simulate the fog neither (Fig. 1c), but it simulates mist, with a decrease in visibility until values between 1 and 5 km close to the surface, approximately at the same time of the observed fog. However, the model overestimates the rest of surface variables during most part of the event (see red thick lines in Fig. 2 and mean biases in Table 4). The overestimation in T_2 , WS_{10} and TKE (quite substantial) seemed to be related to the inability of the model producing more LWC close to the surface until the values needed to produce fog. However, even with these biases in surface variables, this model was able to simulate more realistic conditions of low visibility than WRF.

3.2. Event 2: CBL fog (20 Jan 23:09–21 Jan 01:09 UTC)

3.2.1. Observational description

Fog event 2 (Fig. 3a) is classified as a short-lived (2 h) and deep (> 100 m thickness) CBL fog (Table 3) formed as the result of the descending of low stratus clouds. Visibility lower than 1 km was firstly observed at all the levels above 2 m at 2300 UTC. 30 min later the fog was also observed at the surface level, lasting during 2 h with a thickness of > 100 m. During the next morning, visibility lower than 1 km was observed at the levels of 70 and 100 m around 0700 UTC (see Supplementary Fig. 2a), which could be linked to the CBL formation mechanism of the next fog event (event 3).

Fig. 4 shows the associated surface variables during the event (mean values in Table 3). The deep character of this fog agrees with the relatively high values of TKE (mean of $0.14 \text{ m}^2\text{s}^{-2}$) and the temperature difference between 10 and 2 m (mean of $0.24 \text{ }^\circ\text{C}$), leading to moderate mixing close to the surface (Table 3), which allowed the vertical extension of the fog. T_2 remained higher than the precedent event during the whole fog and pre-fog conditions (around $5\text{--}5.5 \text{ }^\circ\text{C}$, Fig. 4a). A very shallow (1.5–10 m) and weak surface thermal inversion was present, but the temperature remained lower at the levels of 50 and 85 m than at the surface levels. This was caused by the existence of low stratus at higher levels, which dampened the radiative cooling at the surface. The temperature at all the levels increased during the fog event probably due to a warm advection. Mean WS_{10} during the event was 1.73 m s^{-1} , quickly increasing towards the fog dissipation, which was clearly caused by this wind speed increase (Fig. 4b). This event presents

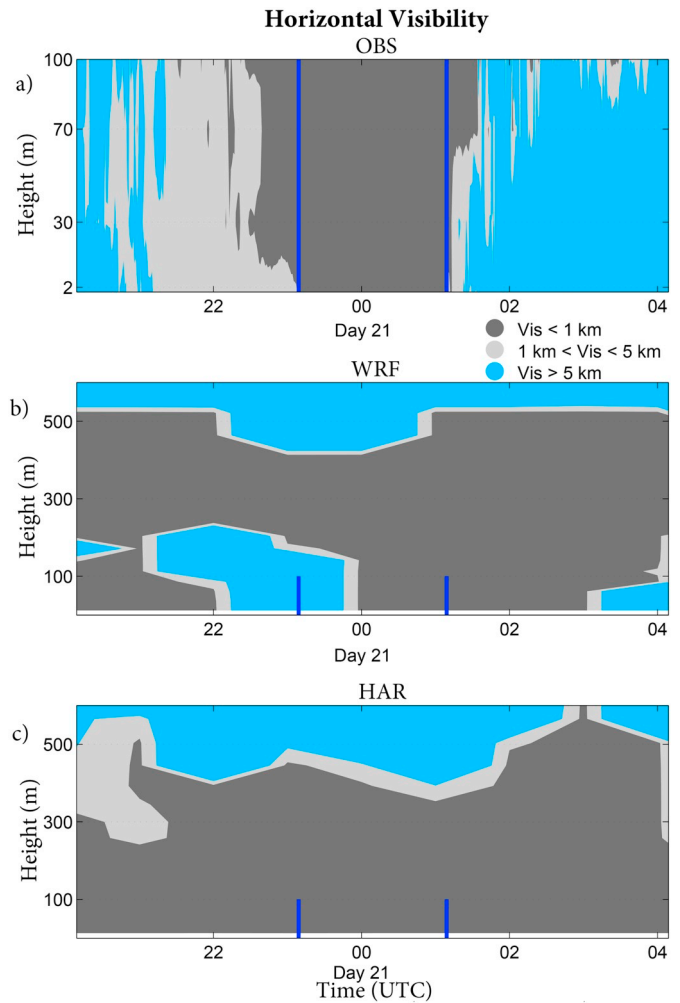


Fig. 3. Idem than Fig. 1 but for event 2, from 20/01 at 2309 UTC to 21/01 at 0109 UTC.

moderate values of TKE (mean of $0.14 \text{ m}^2\text{s}^{-2}$ (Table 3)) and values of almost $0.5 \text{ m}^2\text{s}^{-2}$ during the dissipation stage (Fig. 4d). In contrast to expected and observed in event 1, q_2 (Fig. 4c) did not decrease during the fog event and a weak increase of 0.2 g kg^{-1} was even observed. This was probably due to the commented warm and more humid advection from SW, inferred from synoptical maps (supplemental material 2) and also observed from backward trajectory models (not shown).

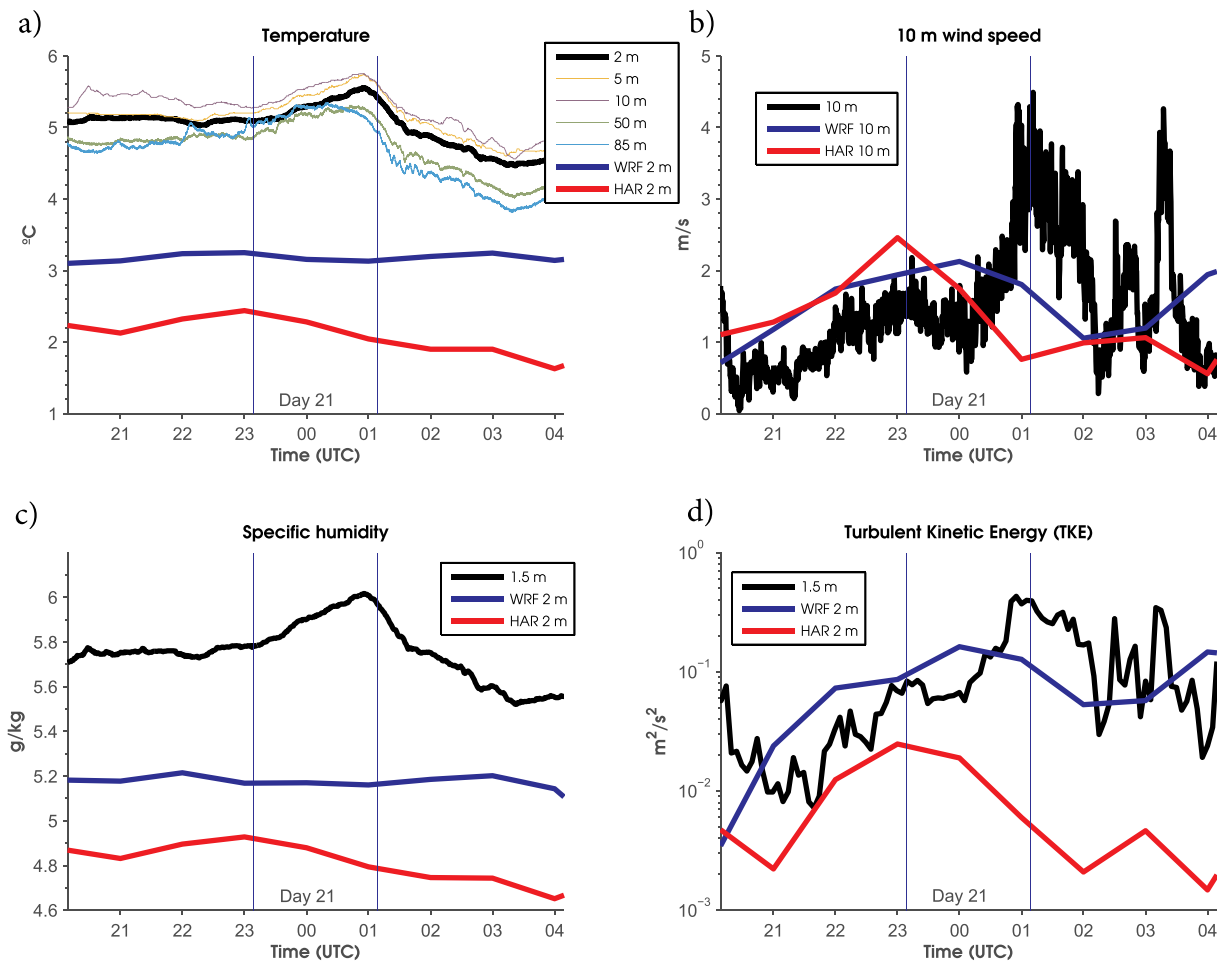


Fig. 4. Idem than Fig. 2 but for event 2, from 20/01 at 2309 UTC to 21/01 at 0109 UTC.

3.2.2. Model skill

Both models clearly overestimate the fog duration (Fig. 3b and c). Since observations are absent above 100 m, the simulated height cannot be evaluated in this case, but the model simulates a fog layer of 400–500 m.

WRF simulates a too-early fog onset (-8 h of bias, see Table 4), although a transitory dissipation is observed close to the surface around 2200 UTC (Fig. 3b) to come back at 0000 UTC, a similar time as the observed fog formation. The CBL mechanism was correctly simulated. The model also simulates the dissipation of the fog during nighttime (2 h later than observed, Table 4) through a transformation into low clouds, which agrees with the observations (Fig. 3b, see also Supplementary Fig. 2b to better observe the post-fog period). Mean biases for the surface variables are shown in Table 4: T_2 is clearly underestimated

by the model (bias of -2.2 °C, see also Fig. 4a), as well as q_2 (-0.76 kg kg^{-1} , Fig. 4c). The underestimation in T_2 also causes enhanced condensation and too high values of LWC, giving rise to a too deep fog. The evolution of WS_{10} is not well simulated, like the observed wind-speed increase around 0100 UTC linked to the dissipation (Fig. 4b, blue line). TKE is slightly overestimated during the pre-fog and first part of the fog, but underestimated at the dissipation stage (Fig. 4d), leading to an overall TKE underestimation (-0.16 m^2s^{-2}) during the fog event.

HARMONIE also simulates a too persistent fog at the surface, clearly overestimating its duration (formation 5 h anticipated and dissipation 10 h delayed, see Table 4). The model also underestimates considerably T_2 and q_2 (see Table 4). WS_{10} and TKE are underestimated during the fog (Table 4) and the observed wind speed and turbulence increases linked to the fog dissipation were not simulated (Fig. 4b). This

underestimation in wind and turbulence avoided the fog dissipation by the model, leading to a too-long event. The skill of HARMONIE simulating these key parameters for fog evolution is, in general, worse than that of WRF in this case.

3.3. Event 3: CBL fog (21 Jan 18:32–23 Jan 10:47 UTC)

3.3.1. Observational description

This event (Fig. 5a) is classified as a CBL fog persisting during almost the whole daytime at the surface with a total duration of over 40 h. The fog was present at all the visibility-measurement levels during a great part of its duration, but it also presents some periods with a thickness lower than 100 m (Fig. 5a). The fog was formed as the result of the lowering of low clouds (Fig. 5a before 1800 UTC of day 21). During the whole event, the fog is only eventually dissipated for short periods close to the surface (2 m) and for that reason, this long event is considered as a unique one. The fog of the previous night (event 2) was converted in low clouds, descending during the day 21 and reaching the ground at 1830 UTC (fog onset). 2-m visibility increased up to values higher than 1 km but lower than 5 km (mist) for short periods during the first night, while the fog was totally dissipated at the surface around 1400 UTC of day 22, but only for a few minutes. The fog behaviour was more irregular during the second night, with observed dissipation at higher levels (for example between 2100 UTC and 0000 UTC, Fig. 5a). Later, the fog was dissipated at all the measurement levels at 0200 UTC approximately. The fog was again observed at 0600 UTC through a new CBL process. Then the fog dissipated completely at 1047 UTC from the layers close to the surface.

Fig. 6 shows the associated surface variables during the event. The mean T_2 was relatively high during this event (mean of 8.76 °C) in comparison with other events (Table 3). The fog onset did not correspond with a progressive surface cooling but with a temperature increasing along the evening previous to the fog formation. The CBL process of fog formation was linked to the observed decrease in WS_{10} before the fog onset (Fig. 6b). The temperature during the fog period continued increasing during the daytime of 22 January, but the temperature could not decrease during the first night with fog (Fig. 6a), due to the thick foggy layer. Finally, the temperature increased after sunrise of day 22 (around 0730 UTC), with the maximum temperature linked to the short-lasting period without fog at the surface at around 1400 UTC.

This fog can be divided into two parts, with the middle of the event in the short-lived dissipation observed around 1400 UTC. The first part of the fog is characterized by relatively high WS_{10} (Fig. 6b), probably associated with a more efficient mixing of the fog (almost always observed at the uppermost visibilimeter at 100 m). WS_{10} during this first part oscillated between 1 and 3 m s^{-1} (Fig. 6b). However, the second part of the fog was characterized by weaker WS_{10} , always $< 1.5 \text{ m s}^{-1}$ and with marked oscillations (Fig. 6b). This could cause the apparition and dissipation of the fog at the surface during this second night since the mixing was not enough to produce a well-developed fog (see Fig. 5a). Regarding the observed turbulence values, the same

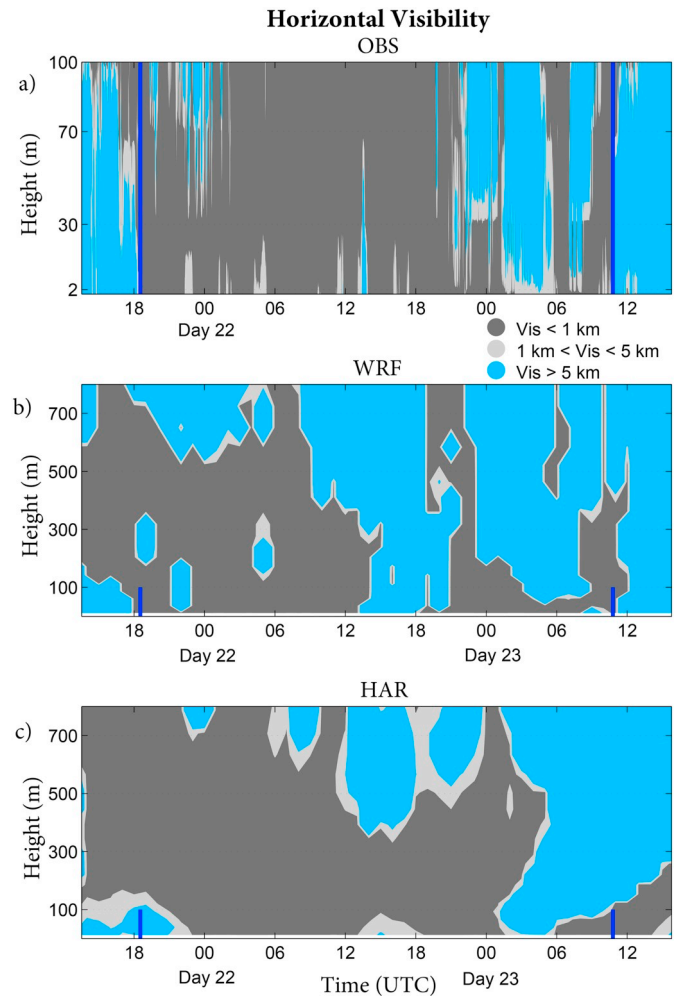


Fig. 5. Idem than Fig. 1 but for event 3, from 21/01 at 1832 UTC to 23/01 at 1047 UTC.

conclusions can be extracted from the analysis of Fig. 6d, with values of the order of $0.1 \text{ m}^2 \text{ s}^{-2}$ during the first part (thicker fog) and $0.01 \text{ m}^2 \text{ s}^{-2}$ during the second part (shallower) of the event, in accordance with results found in Román-Cascón et al. (2016b). On the other hand, the mean q_2 during the event was 7.54 g kg^{-1} with lower values during the first part of the event (Fig. 6c) due to thicker fog and lower visibility values (the fog was denser during this part, visibility values are not shown). However, the second part of the fog was characterized by an increase in q_2 (Fig. 6c) associated with less dense fog (enhanced visibility, less LWC and therefore larger q_2 values).

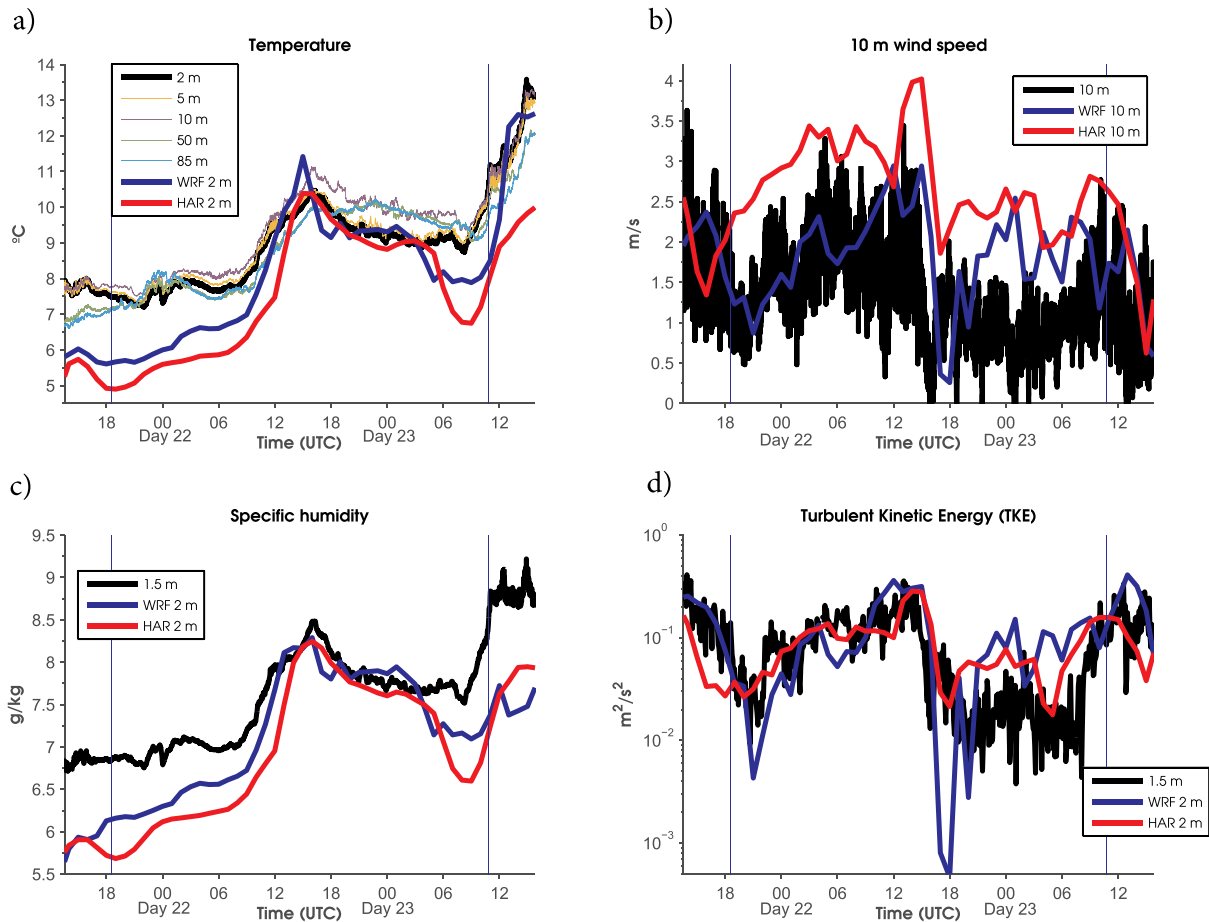


Fig. 6. Idem than Fig. 2 but for event 3, from 21/01 at 1832 UTC to 23/01 at 1047 UTC.

3.3.2. Model skill

WRF simulates relatively well the fog onset following a CBL process and also the fog dissipation for this long-lasting fog event (Fig. 5b, onset bias of -1 h and dissipation bias of $+1$ h, see Table 4). The surface dissipation observed during the day 22 at 1400 UTC is well captured by the model, but its duration is overestimated (it lasts a few minutes in the observations and 4.5 h in the model). Besides, the model dissipates the fog at all levels while this short dissipation only extended up to the 30-m level according to the observations (Fig. 5a). The process of final dissipation is also quite well simulated by the model, including the cloud structures formed in the lowest layers (it cannot be evaluated above 100 m agl). Globally, the WRF model simulates correctly this event, except for the overestimation in the duration of the fog dissipation in the middle of the event. Regarding the fog thickness, the model simulates a fog layer of 300–800 m during the first part and 50–400 m fog during the second part of the event. It is impossible to

evaluate the fog thickness with the available data, however, the tendency of thickness decreasing agrees with the observations.

HARMONIE also simulates a CBL process associated with the fog formation, but delaying the fog onset and dissipation (Fig. 5c, onset bias of $+4$ h and dissipation bias of $+4$ h, see Table 4). In this case, HARMONIE is able to simulate correctly the fog during the daytime, only with a short surface dissipation that agrees well with the observations (slightly delayed). The model also simulates satisfactorily the fog dissipation process, even the observed temporal dissipation at the surface from 0200 UTC to 0600 UTC. The simulated fog thickness is in accordance with those simulated by WRF, with thicker fog during the first part of the fog and shallower (although thick) during the second part of the fog. The overestimation in fog thickness is greater by HARMONIE than by WRF during the second part of the event.

T_2 and q_2 are underestimated by both models (especially by HARMONIE) during most part of the fog event, especially during the first

part of the fog (Fig. 6a and c). In any case, the evolution of both simulated variables agrees well with the observations. The simulation of WS_{10} (Fig. 6b) by WRF agrees well with the observations, but it is systematically overestimated by HARMONIE (mean bias of $+1.29 \text{ m s}^{-1}$). TKE is correctly simulated by WRF and HARMONIE during the first part of the event and slightly overestimated during most part of the second part (Fig. 6d), except for an important TKE decrease simulated by WRF at 1800 UTC of day 22, observed at the same time that the fog dissipation simulated by the model.

3.4. Event 4: radiation fog (23 Jan 19:29–24 Jan 08:24 UTC)

3.4.1. Observational description

Fog event 4 (Fig. 7a) is a long (12.9 h) radiation fog with variable thickness (mean of 40 m). The fog was only observed at the surface level (2 m) for more than 4 h (Fig. 7a). At midnight, the fog started growing in the vertical, reaching 100 m from 0030 UTC to 0130 UTC. The thickness of the fog decreased later and during the rest of the night it oscillated between 2 and 30 m. The fog was dissipated from surface 1 h after sunrise (which occurred at 0730 UTC).

As in a pure radiation fog, the fog formation was the result of the decreasing surface temperature, from 13°C at 1630 UTC to 8°C at 1930 UTC (fog formation) (Fig. 8a). The pre-fog surface-based thermal inversion was maintained during the first very-shallow part of the fog (until 0000 UTC). Then the fog grown vertically associated with the turbulent mixing increase (more than one order of magnitude), causing the temperature homogenization at all the levels (increasing at lower levels and decreasing at higher ones, Fig. 8a at 0130 UTC). Afterwards, the temperature at different levels diverged and the inversion was formed again, with nighttime surface radiative cooling despite the presence of the fog layer. After the fog dissipation, a quick temperature increase was observed linked to the initiation of the daytime convection. The mean $T_{10} - T_2$ during the whole fog was 0.98°C , showing the characteristics of shallow and not-well mixed fog events, associated with low values of TKE (mean of $0.04 \text{ m}^2\text{s}^{-2}$). However, for a short period of time it also showed the characteristics of well-mixed deeper fogs: temperature convergence, TKE up to $0.1 \text{ m}^2\text{s}^{-2}$ and thickness of $> 100 \text{ m}$. Despite its mostly shallow character, the mean WS_{10} during this event was the highest observed among all the six analysed events (see Table 3), with 1.80 m s^{-1} of mean and some periods with WS_{10} higher than 2.5 m s^{-1} (at 0100 UTC, Fig. 8b), linked to the fog vertical extension. Visibility values (not shown) were extremely low (30–40 m of visibility) when the fog was observed at all the levels (0000–0200 UTC). However, values of around 1 km of visibility were observed during the first part of the very shallow fog and intermediate values in the second part, when the fog presented a thickness of between 30 and 70 m. Therefore, a relation between fog thickness and visibility is clearly observed in this event: the thicker the fog, the more dense it was. q_2 was continuously decreasing during the event (Fig. 8c),

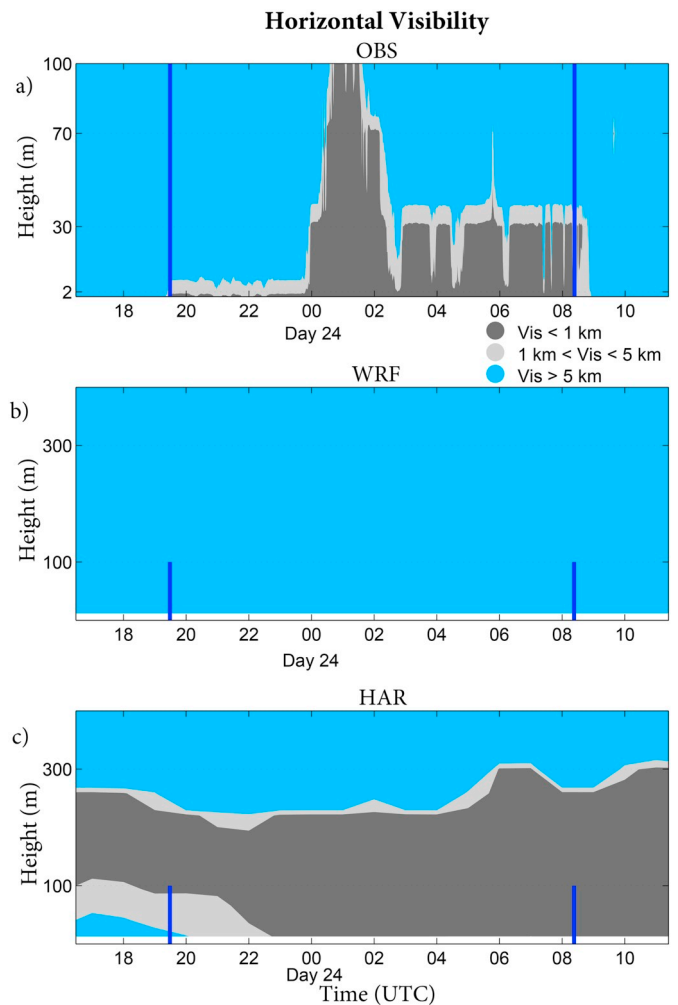


Fig. 7. Idem than Fig. 1 but for event 4, from 23/01 at 1929 UTC to 24/01 at 0824 UTC.

with pre-fog values decreasing from 9 to 7 g kg^{-1} in 3 h and still decreasing during the event to $< 5 \text{ g kg}^{-1}$ at the end of the event. The significant increase in q_2 observed after the fog dissipation suggests that these important variations in atmospheric humidity were due to the condensation/evaporation processes associated with the fog. This event presents the largest variations in q_2 compared to all the analysed events, and are related to the punctual very low values of visibility reached in some cases. In fact, the increase in q_2 observed at 0100 UTC was due to

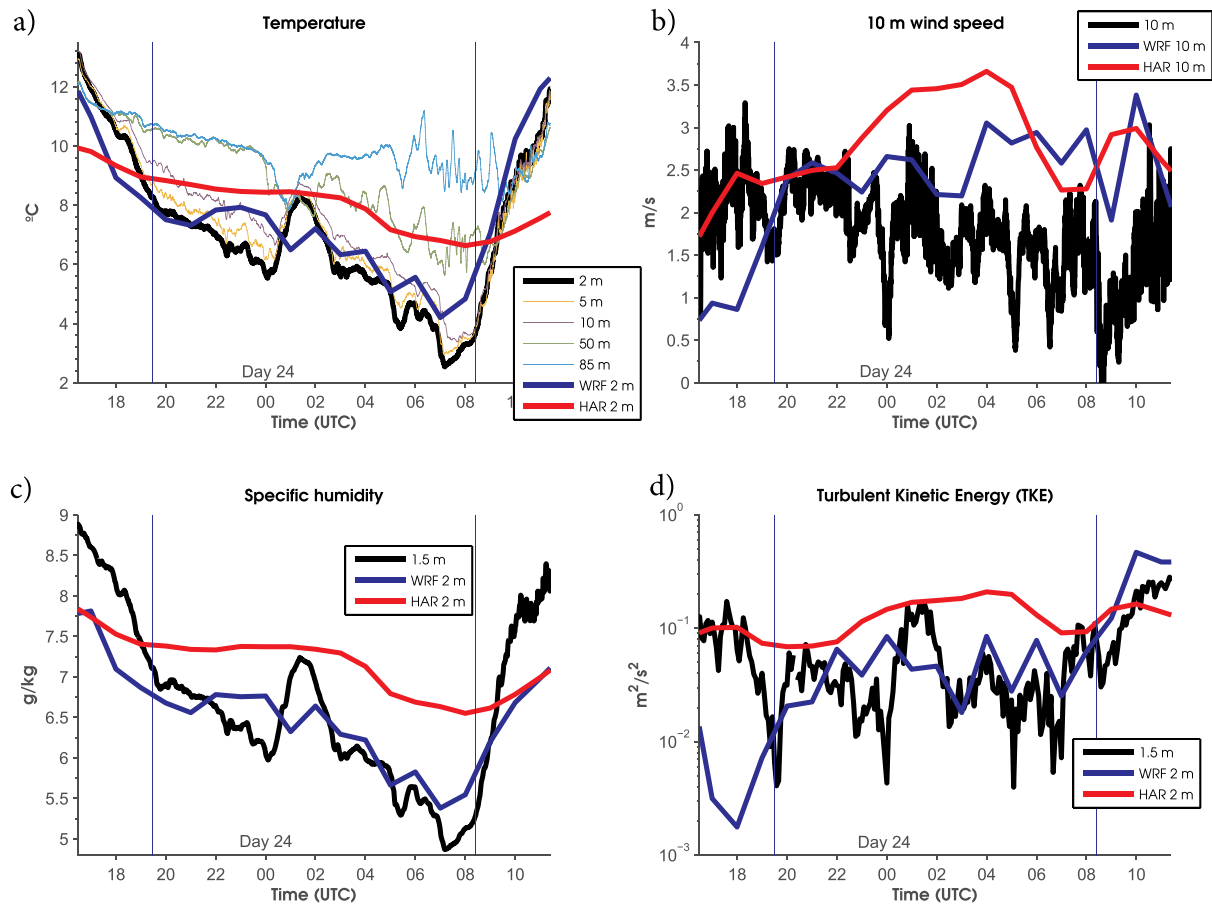


Fig. 8. Idem than Fig. 2 but for event 4, from 23/01 at 1929 UTC to 24/01 at 0824 UTC.

enhanced mixing between the surface-fog layer (with less q_2) and air from upper layers (warmer and with relatively high q_2). In these upper layers, the fog was not formed earlier, maintaining their original air humidity values, i.e., without losing water vapour due to condensation. The mean TKE during the fog was $0.04 \text{ m}^2\text{s}^{-2}$ (Table 3); however, values of up to $0.1 \text{ m}^2\text{s}^{-2}$ were observed between 0000 UTC and 0200 UTC (Fig. 8d), favouring the fog vertical extension.

3.4.2. Model skill

The WRF model was unable to simulate this fog event at all (Fig. 7b). However, the model was able to simulate quite correctly the surface variables, including the T_2 decreasing (Fig. 8a, blue thick line),

with a slight positive bias of $+0.58 \text{ }^\circ\text{C}$ during the fog event (Table 4). WS_{10} was overestimated by the model (bias of $+0.79 \text{ m s}^{-1}$), but the turbulence was in general quite well simulated (no bias in TKE , Fig. 8d). The model was even able to simulate the significant q_2 decrease observed during the whole event (Fig. 8c). However, despite the general correct simulation of these key surface variables, the LWC simulated by the model from surface to 300 m agl remained quite low, with no fog nor mist formation. We think that the modelled decrease in q_2 should be due to condensation due to its similarity to the observations. However, the relatively high values of wind (this was the event with higher wind speed) in addition to the model overestimation of $+0.79 \text{ m s}^{-1}$ could contribute to the unsuccessful formation of fog. Besides, additional

issues related with the microphysics scheme could contribute to the inability of the model for the simulation of this event.

The HARMONIE model simulated a fog layer of 200 m formed as the result of the lowering of low clouds of the previous event 3 (Fig. 7c). In fact, the formation mechanism is different from the real one, but the model simulates a fog formed at 2300 UTC (later formation, +3 h of bias) and too-late dissipated at 1200 UTC (4 h delayed). Besides, the simulated fog has a thickness of > 200 m, while a shallower fog was observed with the visibilimeters during most part of the event. The surface-radiative cooling was limited in the HARMONIE model (Fig. 8a, red thick line) due to the simulation of low clouds during the whole previous day. This leads to a global fog-event overestimation of +2.04 °C (Table 4). WS_{10} and TKE were also clearly overestimated (+1.29 °C and almost 0.1 m²s⁻² respectively), as well as q_2 (almost 1 g kg⁻¹). That is, the model was able to simulate some fog during the period, but for incorrect reasons and through the incorrect mechanisms, influencing the biases found in surface variables.

3.5. Event 5: radiation fog (26 Jan 02:53–26 Jan 09:34 UTC)

3.5.1. Observational description

This case is a very shallow (thickness of 27 m) radiation fog lasting for 6.7 h (Fig. 9a). No fog was observed the day before this event, maybe due to the passage of a front linked to the synoptic trough at the west of the Iberian Peninsula (Supplementary Fig. 1f). However, this event formed even with colder air at higher heights (Supplementary Fig. 1g). The fog was formed due to the radiative cooling during the first night of day 26 January (Fig. 10a); it remains very shallow during a great part of the event, only observed at the first level with observations (2 m) and extending up to the second level (30 m) for some moments (Fig. 9a). The visibility was lower than 1 km at 70 and 100 m levels only during very short periods. The very shallow character of this fog is in accordance with the strong surface-based thermal inversion observed (mean of 1.81 °C of difference between 10 and 2 m, the maximum inversion in comparison with all the events, Table 3) and with the very low values of WS_{10} and TKE (mean of 1.17 m s⁻¹ and 0.03 m s⁻¹ respectively, Table 3), being also the lowest mean WS_{10} and TKE values in comparison with the other events.

A thermal inversion was present during the pre-fog period and also during the fog (Fig. 10a), with near-surface temperature decreasing during the night despite the fog presence. Some homogenization in the surface temperatures was only observed after sunrise (which occurred at approx. 0730 UTC), associated with the after-sunrise mixing and fog dissipation process. Although WS_{10} and TKE remained low during the event (Fig. 10b and d), the fog thickness (Fig. 9a) was quite sensitive to sporadic changes in these variables, as observed for example around 0600 UTC. The dissipation of the fog was observed with low values of WS_{10} and was caused by the increase in surface temperature and TKE

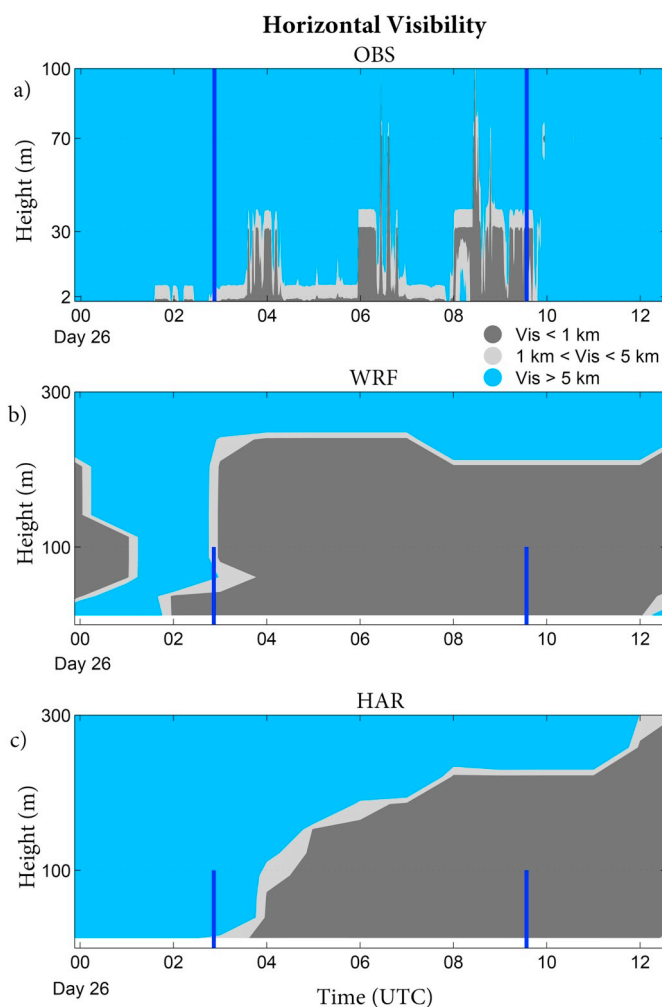


Fig. 9. Idem than Fig. 1 but for event 5, from 26/01 at 0253 UTC to 26/01 at 0934 UTC.

after sunrise (Fig. 10a and c). The q_2 decrease observed during the pre-fog and first part of the fog event was linked to the condensation process (Fig. 10c) while the increase observed in the last stage of the fog event was linked to the mixing of surface levels with air from above, as well as to the droplets evaporation processes associated with the fog dissipation stage.

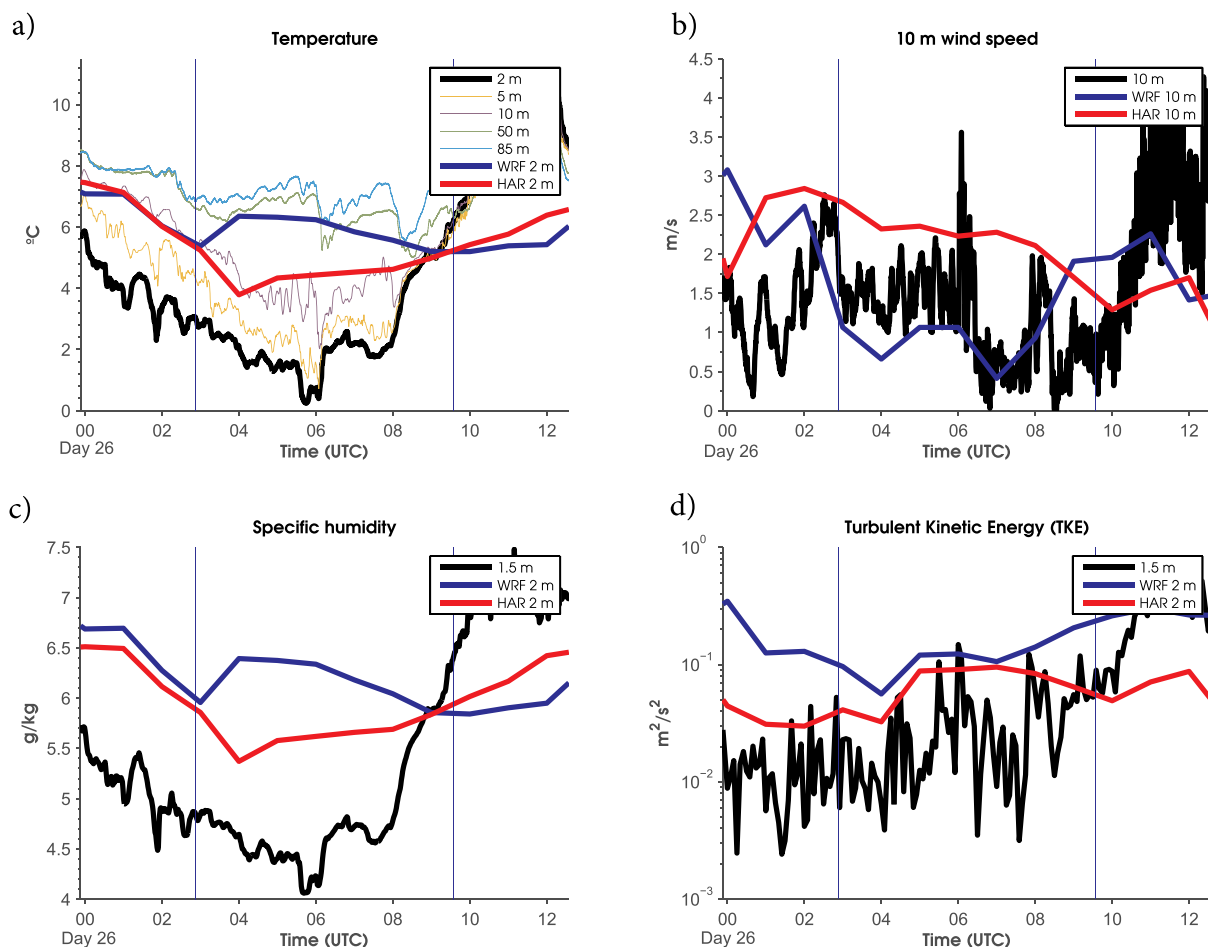


Fig. 10. Idem than Fig. 2 but for event 5, from 26/01 at 0253 UTC to 26/01 at 0934 UTC.

3.5.2. Model skill

WRF simulates a radiation fog event firstly formed at the surface about 1 h before the real formation (Fig. 9b). Then it simulates a fog growing in the vertical up to > 200 m and lasting until midday (dissipation 2.5 h delayed regarding the observations, see Table 4). The model clearly overestimates the fog thickness. With respect to the

simulation of surface variables, WRF overestimates T_2 during most part of the event, with a remarkable mean bias of $+3.35\text{ }^\circ\text{C}$ (unable to simulate the surface cooling). It also overestimates q_2 ($+1.35\text{ g kg}^{-1}$). This higher content in surface air humidity allowed the condensation process (fog formation) even with higher simulated values of surface temperature. The model slightly underestimates WS_{10} but

overestimates TKE , giving rise to exaggerated vertically extended fog.

The HARMONIE model simulates a similar fog as WRF but slightly delayed in time (Fig. 9c). This model also overestimates T_2 and q_2 , with slightly lower (but still significant) bias than WRF ($+2.06^\circ\text{C}$ and $+0.85\text{ g kg}^{-1}$ respectively, Fig. 10a and c). However, in this case, the WS_{10} was overestimated during most part of the event (mean bias of $+0.85\text{ m s}^{-1}$), in contrast to WRF (Fig. 10b). Due to the incorrect later dissipation in both models, the temperature is underestimated after the observed fog dissipation stage around 0900 UTC (Fig. 10a).

3.6. Event 6: CBL fog (26 Jan 21:21–27 Jan 10:16 UTC)

3.6.1. Observational description

This event is a thick ($> 100\text{ m}$ during most part of the period) CBL fog of long duration (13 h, Fig. 11a). Additional visibility and long-wave radiation measurements (not shown) from the previous day showed how some low clouds were observed during the day 26 after the morning dissipation of event 5. The fog was formed at 2121 UTC as the result of the lowering of low-cloud bases (Fig. 11a). The fog was firstly observed at all the levels with measurements and then converted into a shallow fog for some time around 0000 UTC, to be extended in the vertical up to (at least) 100 m after 0130 UTC. The final dissipation was observed from the surface well after sunrise and the fog was subsequently transformed into low clouds the following daytime. The mean temperature difference between 10 and 2 m was low (0.20°C), associated with relatively high values of turbulence (mean TKE of $0.11\text{ m}^2\text{s}^{-2}$), leading to the observed thick fog. This weak stratification fulfils the expected features of deep fog (Román-Cascón et al., 2016b).

As observed in the temperature records (Fig. 12a), no surface-based thermal inversion existed before the fog formation and the temperature was well homogenized at all the levels during most part of the event. Only a short period around 0000 UTC showed a temperature decoupling between the surface and higher levels (50 and 85-m) (Fig. 12a), associated with the shallow fog observed in that period. WS_{10} was lower than 2 m s^{-1} also during most part of the event except for the period from 0030 UTC to 0200 UTC. Like in CBL-fog event 3, WS_{10} decreased during the afternoon allowing the fog formation through a CBL mechanism (Fig. 12b). From 0030 UTC to 0200 UTC, WS_{10} increased up to $> 3\text{ m s}^{-1}$ (reaching even values of 5 m s^{-1}), which caused the fog dissipation at several heights except at the lowest level of 2 m. A similar increase in WS_{10} was observed at the dissipation stage (Fig. 12b). Turbulence values remained around $0.04\text{ m}^2\text{s}^{-2}$ during the whole event, helping the fog vertical extension. However, the excess in turbulence observed around 0200 UTC ($0.2\text{--}0.4\text{ m}^2\text{s}^{-2}$, note the high values) did not contribute to the fog vertical extension but to its partial

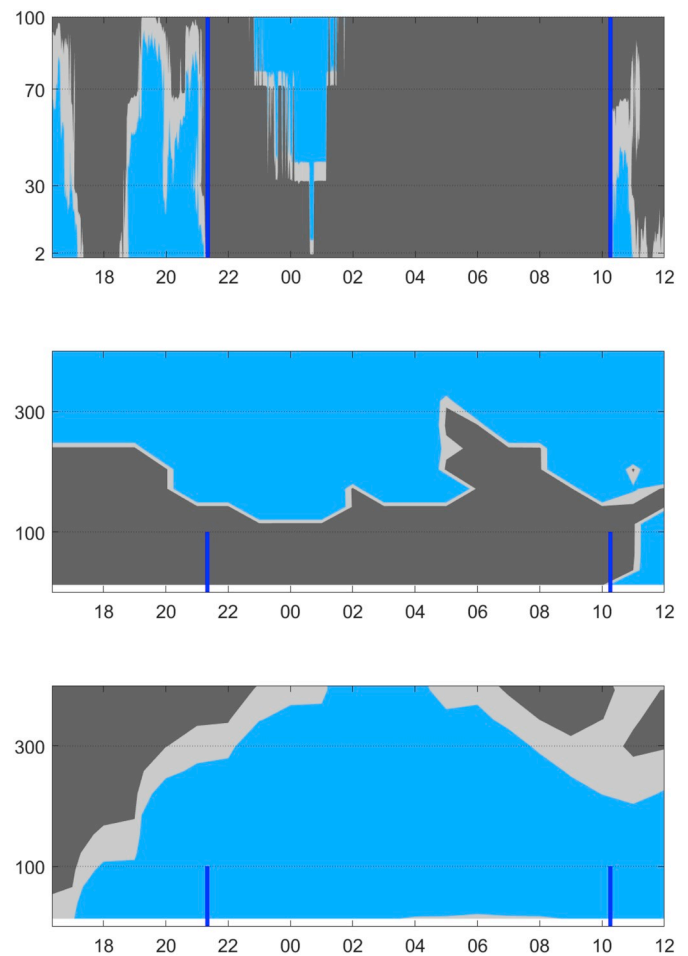


Fig. 11. Idem than Fig. 1 but for event 6, from 26/01 at 2121 UTC to 27/01 at 1016 UTC.

dissipation (Fig. 12d). q_2 behaviour was linked to the temperature evolution, decreasing from 2000 UTC to 0100 UTC (related to the condensation process linked to the fog formation Fig. 12c). This variable also showed temperature-dependent oscillations during the rest of the event, as expected when saturation values of relative humidity are reached.

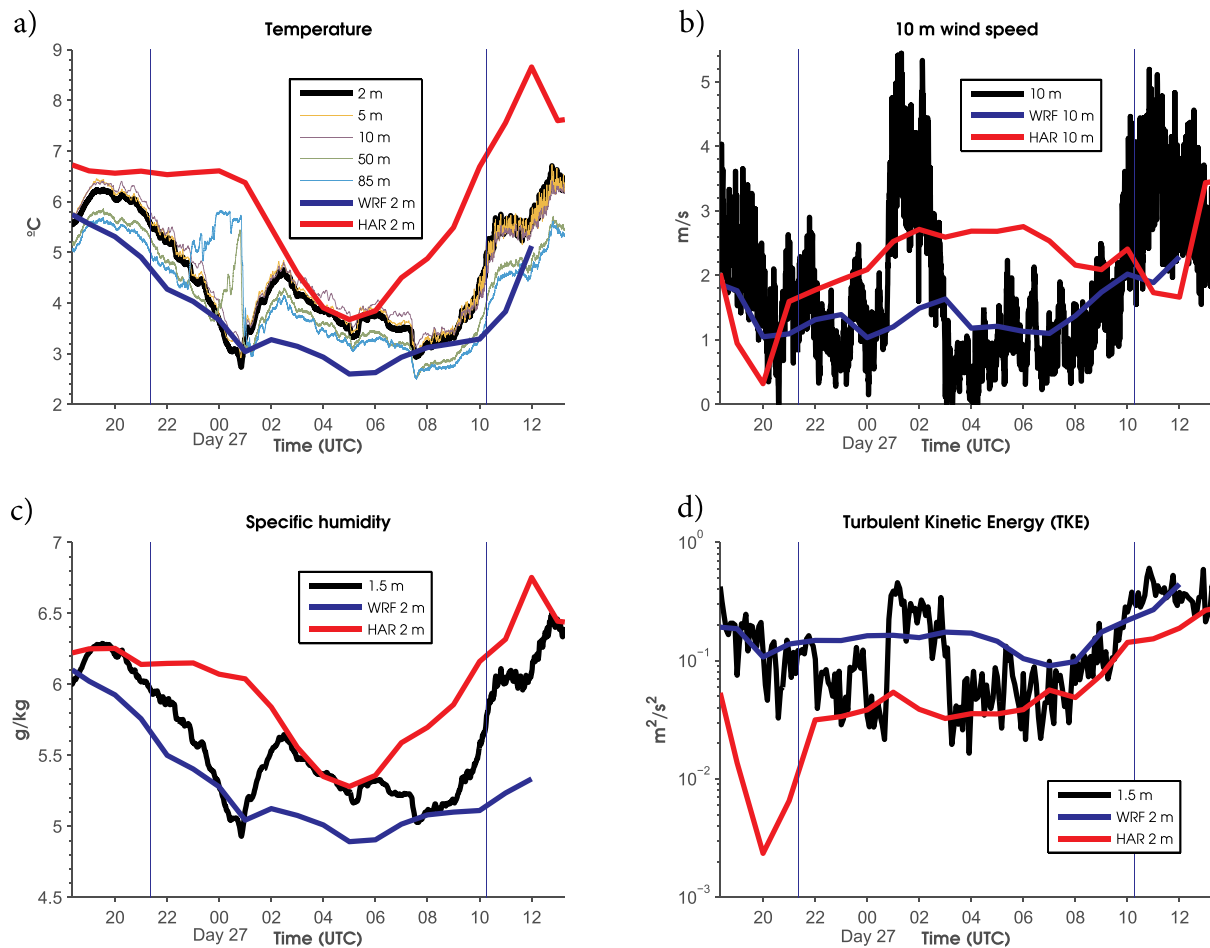


Fig. 12. Idem than Fig. 2 but for event 6, from 26/01 at 2121 UTC to 27/01 at 1016 UTC.

3.6.2. Model skill

WRF simulates basically the continuation of the fog event 5 (Fig. 11b and Supplementary Fig. 2b). Thus, it fails in the cloud-base lowering formation mechanism giving rise to this fog. However, the simulated fog has a thickness of 100–200 m which could be in accordance with the observations. The model also simulates a quite correct fog dissipation from the surface (+1 h of bias). The simulation of T_2 and WS_{10} is acceptable, except during the period around 0000 UTC when the fog was dissipated at higher heights due to the significant observed wind increase (not simulated). TKE was overestimated during the whole fog event except during the period of this commented dissipation.

The HARMONIE model is not able to simulate the fog during this period (Fig. 11c and Supplementary Fig. 2c); it only simulates low clouds which were a continuation of event 5. The simulation of these low clouds damped the observed evening surface cooling (Fig. 12a). Thus, the model shows a mean positive T_2 bias of +1.41 °C (Table 4). The model also overestimate WS_{10} during most part of the period (Fig. 12b) but not TKE, which simulation is quite correct (Fig. 12d). Regarding q_2 , the model simulates appropriately the range of values, but it is not able to simulate the observed q_2 decrease from 2000 UTC to 0100 UTC.

4. Discussion of model results

From the analysis shown in Section 3, we can state that during this period and in this area, the simulation of radiation fog is more challenging than CBL ones for these two mesoscale models. In order to illustrate the general model skill, Fig. 13a shows the models hit rate for the simulation of radiation and CBL fog. This performance indicator is calculated attending to the fog occurrence at each hour (total period of 192 h), which is based on visibility measurements (observations) and in LWC output converted to visibility (models). As commented in Section 2, fog is in both cases considered when the visibility is lower than 1000 m at the lowest level. The radiation-fog hit rate is quite low for WRF (30%, it missed two events), while it is higher (75%) for HARMONIE. The results for CBL fog are different, WRF has a high hit rate of 90%, while the HARMONIE hit-rate only reaches 50%, in part due to the missing of CBL fog event 6 and to biases in the onset and dissipation times of the events. These results show important differences on the model skill depending on the fog-formation mechanism. The model difficulties for the simulation of the radiative cooling at the surface plays a key role to simulate radiation fog. In fact, in some cases, this is caused by the overestimation in duration and thickness of CBL fog (or low clouds) the previous day. That is, if the model simulates an

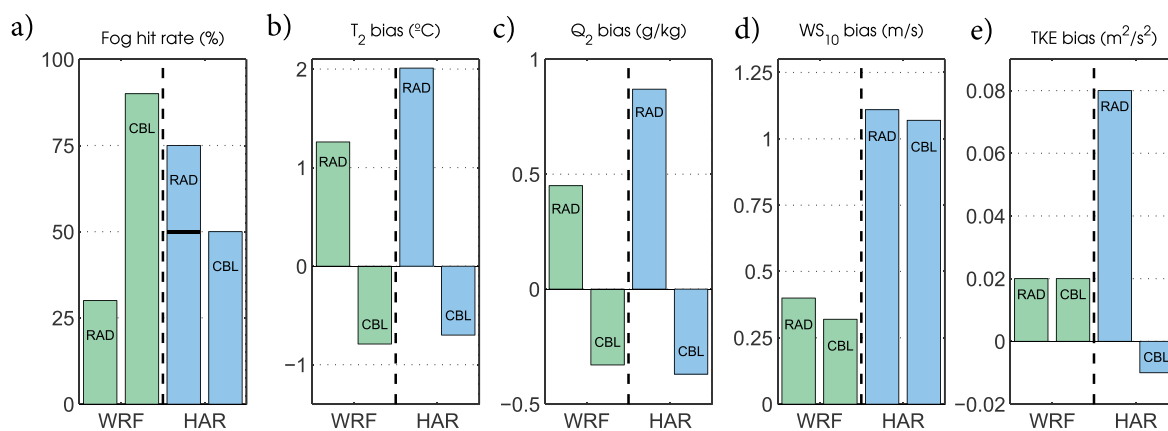


Fig. 13. WRF (green) and HARMONIE (blue) model skill (hourly basis) for radiation and CBL fog. (a) Hit rate (% of hours) simulating the observed fog. Small black horizontal line in radiation fog by HARMONIE is the result without event 4, which was simulated but following an incorrect mechanism of formation; (b) T_2 bias ($^{\circ}\text{C}$); (c) q_2 bias (g kg^{-1}); (d) WS_{10} bias (m s^{-1}); (e) TKE bias (m^2s^{-2}). (For interpretation of the references to colour in this figure legend, the reader is referred to the web version of this article.)

overestimated CBL fog (in thickness and duration), the modelled surface cooling of the next night can be limited by the low-clouds. This effect is observed, for example, for HARMONIE in radiation fog event 1 (Figs. 1c and 2a) and event 4 (Figs. 7c and 8a) and for WRF in event 5 (Figs. 9c and 10a).

On the other hand, the total false alarm ratio (hourly basis) was approximately similar for both models (29% for WRF and 28% for HARMONIE). Note how the evaluation of the false alarm ratio regarding the fog formation mechanism is not possible, since it takes into account periods without observed fog (therefore, the determination of fog type is not possible). Related to this, we have compared the observed and simulated hours of fog (Table 5). At the surface level, the observed visibility was below 1 km during 60 h while the models tend to overestimate the fog simulation (82 and 72 h for WRF and HARMONIE respectively). That is, the models have a tendency to produce too much fog, even despite their inability to simulate some fog events. This result of fog overforecasting agrees with previous findings of works comparing both models (Fernández-González et al., 2019), although they found slightly better skill for HARMONIE than WRF. In any case, the site and the type of the analysed fog events differ from those of this study. Table 5 also shows the number of hours with visibility lower than 1 km observed at 100 m agl (50 h), in comparison with a similar height in the models (88 h for each one). This means that it was more common to observe fog (at 2 m) than low visibility (fog or low clouds) at 100 m agl during the analysed period. However, for the models a tendency exists towards a more frequent simulation of low visibility at around 100 m than at the surface. This comparison clearly illustrates the tendency of models to vertically overestimate fog, in many cases also observed at around 200 m agl (see Table 5). This tendency is slightly larger for HARMONIE than for WRF, in accordance with previous

Table 5

Number of hours with visibility lower than 1 km from a total of 192 h analysed at three different levels. Observation levels are 2 and 100 m (no visibilimeter above). WRF levels are 13, 113 and 204 m. HARMONIE levels are 13, 113 and 220 m. Modelled and observed hours differences are also included with percentages of overestimation between brackets. The 200-m level is included to show the model tendency to extend the fog in the vertical.

	Hours with vis < 1 km		
	Lowest level	~ 100 m	~ 200 m
OBS	60 h	50 h	//
WRF	82 h (+36%)	88 h (+76%)	77 h
HAR	72 h (+20%)	88 h (+76%)	87 h

studies comparing both models (Steenefeld et al., 2015).

Now we link these results to the biases in fog-related near-surface variables. The models systematically overestimate T_2 during the radiation fog events (Fig. 13b). Despite the better skill of HARMONIE for the simulation of this type of fog, the T_2 bias is larger ($+1.98^{\circ}\text{C}$) than for WRF (1.26°C). The positive biases indicate the inability of the models to simulate the real radiative cooling at the surface associated with radiation fog conditions. However, the T_2 biases are negative and smaller in absolute values during the CBL fog events, which are in general better simulated. The biases of q_2 (Fig. 13c) are linked to those of T_2 ; the positive biases during radiation fog indicate the inability of the model to condensate enough water vapour into LWC, due to too high simulated temperatures. On the contrary, both models underestimate q_2 during CBL fog, linked also to the underestimation of T_2 for this type of fog (and to an overestimation of LWC and fog thickness). On the other hand, there is a general overestimation of WS_{10} (Fig. 13d) for both radiation and CBL fog. The bias is substantially larger for the HARMONIE model than for WRF, as occurs also for TKE (Fig. 13e). In any case, the global results for TKE and wind should be analysed with caution, since in the event-by-event analysis we discussed how sudden and unexpected TKE and WS_{10} increases and decreases are typically observed and normally not simulated by the models at the time of occurrence. This is another important weakness of models, since these sudden changes influence the evolution of the fog.

5. Summary and conclusions

A period of 8 consecutive days composed by alternating radiation (3 events) and cloud-base lowering (CBL) (3 events) fog has been analysed observationally at the CIBA site in Spain. This period was characterized by relatively calm and stable conditions over the Iberian peninsula. We find a relatively high event-by-event variability of fog characteristics. However, the specific features of radiation and CBL fog are distinguished. The radiation fog events were associated with colder and drier near-surface conditions than CBL ones (2.5°C versus 6°C and 4.9 g kg^{-1} versus 6.3 g kg^{-1} for radiation and CBL fog respectively). The TKE values were significantly lower during radiation ($0.04\text{ m}^2\text{s}^{-2}$) than during CBL fog ($0.11\text{ m}^2\text{s}^{-2}$), associated with stronger surface-based temperature inversions (mean $T_{10} - T_2$) in radiation fog (1.14°C) in comparison with CBL fog (0.31°C). These differences in stability affected the differences in mean fog thickness for radiation (33 m) and CBL fog (normally $> 100\text{ m}$). However, these differences in TKE were not observed in WS_{10} . That is, radiation fog is observed with low values of TKE compared to CBL fog but the same was not observed in WS_{10} , which highlights the importance of turbulence in fog evolution. The

specific humidity evolution was linked to the temperature changes along the fog event, as expected in conditions of saturated air. The fog thickness (and also the dissipation) showed high sensitivity to small changes in wind speed and turbulence, but particularly in radiation fog.

Subsequently, we have evaluated the fog-forecasting ability of two mesoscale models (WRF and HARMONIE) set up with a similar configuration. Both models exhibited greater difficulties in forecasting radiation fog than CBL fog. For radiation fog, their inability to reach low surface temperature affected the fog simulation, except in some cases when the saturation conditions were well simulated but not the fog, specially for the WRF model. In several cases, the incorrect simulation of previous low-stratus clouds or CBL fog (too thick and/or too extended in time) avoided the real surface radiative cooling needed to simulate radiation fog observed during the next nighttime. That is, under this period with alternating CBL and radiation fog, the models have special difficulties due to this issue, since they normally overestimate the thickness of fog, causing delayed dissipations (+ 1.75 h in WRF and + 5.25 h in HARMONIE) and too long events.

The hit rate for radiation fog was higher for HARMONIE (75%) than for WRF (30%), although only one from three radiation fog events was simulated correctly by both models. For CBL fog, the models had fewer problems, with a hit rate of 90% for WRF and 50% for HARMONIE. The event which was better simulated by both models was the long-lasting and persistent CBL fog event 3, which was the longest and most persistent one. Shallow and shorter fog events were more challenging for the models. Regarding the simulation of key surface variables during the fog events, the WRF model presented smaller biases than HARMONIE, although in some cases this did not improve the simulation of fog. Moreover, in some radiation-fog events the WRF model showed an appropriate simulation of surface variables (temperature, specific humidity, wind and turbulence) but no fog at all.

This work shows how NWP models still need to be improved to reach acceptable fog forecasting. In particular, they need to avoid the exaggerated vertical extension and duration of CBL fog (and also low clouds) that influence the surface cooling needed to simulate the formation of radiation fog events formed during the next night. They also need to take into account processes (which are probably sub-grid scale processes or mesoscale phenomena not well simulated) that can generate turbulence or increase the wind speed during the night, since the fog (especially radiation fog) is highly influenced by these changes that are normally not simulated by the models. In any case, sensitivity analyses of different model schemes and parameterizations (as for example done in Wilson and Fovell (2018)) can also help providing us more insight about the specific changes needed in models to simulate some of the most difficult cases, like the shallow radiation fog events.

Supplementary data to this article can be found online at <https://doi.org/10.1016/j.atmosres.2019.06.018>.

Acknowledgements

This research has been funded by two Spanish National Projects [Ref. CGL2012-37416-C04-02 (MINECO/FEDER) and Ref. CGL2015-65627-C3-3-R (MINECO/FEDER)]. Jon A. Arrillaga is supported by the Predoctoral Training Program for No-Doctor Researchers of the Department of Education, Language Policy and Culture of the Basque Government (PRE_2017_2_0069, MOD = B). Thanks to ECMWF for providing the data for the initialization of the models. We thank www.meteociel.com and NCEP for the reanalysis maps shown in the supplementary material.

References

- Azevedo, J., Morgan, D., 1974. Fog precipitation in coastal California forests. *Ecology* 55 (5), 1135–1141.
- Bari, D., Bergot, T., El Khilfi, M., 2015. Numerical study of a coastal fog event over Casablanca, Morocco. *Q. J. R. Meteor. Soc.* 141 (690), 1894–1905.
- Bartok, J., Bott, A., Gera, M., 2012. Fog prediction for road traffic safety in a coastal

- desert region. *Bound.-Layer Meteorol.* 145 (3), 485–506.
- Bengtsson, L., Andrae, U., Aspelien, T., Batrak, Y., Calvo, J., de Rooy, W., Gleeson, E., Hansen-Sass, B., Homleid, M., Hortal, M., et al., 2017. The HARMONIE-AROME model configuration in the ALADIN-HIRLAM NWP system. *Mon. Weather Rev.* 145 (5), 1919–1935.
- Bergot, T., Apr 2013. Small-scale structure of radiation fog: a large-eddy simulation study. *Q. J. R. Meteorol. Soc.* 139 (673), 1099–1112. <http://doi.wiley.com/10.1002/qj.2051> <https://doi.org/10.1002/qj.2051>.
- Bergot, T., Guedalia, D., 1994. Numerical forecasting of radiation fog. Part I: Numerical model and sensitivity tests. *Mon. Weather Rev.* 122 (6), 1218–1230.
- Bergot, T., Terradellas, E., Cuxart, J., Mira, A., Liechti, O., Mueller, M., Nielsen, N.W., 2007. Intercomparison of single-column numerical models for the prediction of radiation fog. *J. Appl. Meteorol. Climatol.* 46 (4), 504–521.
- Boutle, I., Finnenkoetter, A., Lock, A., Wells, H., 2016. The London model: forecasting fog at 333 m resolution. *Q. J. R. Meteorol. Soc.* 142 (694), 360–371.
- Chaouh, N., Temimi, M., Weston, M., Ghedira, H., may 2017. Sensitivity of the meteorological model WRF-ARW to planetary boundary layer schemes during fog conditions in a coastal arid region. *Atmos. Res.* 187, 106–127.
- Cornejo-Bueno, L., Casanova-Mateo, C., Sanz-Justo, J., Cerro-Prada, E., Salcedo-Sanz, S., 2017. Efficient prediction of low-visibility events at airports using machine-learning regression. *Bound.-Layer Meteorol.* 165 (2), 349–370.
- Cuxart, J., Yagüe, C., Morales, G., Terradellas, E., Orbe, J., Calvo, J., Fernández, A., Soler, M., Infante, C., Buenestado, P., et al., 2000. Stable atmospheric boundary-layer experiment in Spain (sables 98): a report. *Bound.-Layer Meteorol.* 96 (3), 337–370.
- Dawson, T.E., 1998. Fog in the California redwood forest: ecosystem inputs and use by plants. *Oecologia* 117 (4), 476–485.
- Dupont, J.-C., Haeffelin, M., Protat, A., Bouniol, D., Boyouk, N., Morille, Y., 2012. Stratus-fog formation and dissipation: a 6-day case study. *Bound.-Layer Meteorol.* 143 (1), 207–225.
- Dupont, J.-C., Haeffelin, M., Wærsted, E., Delanoe, J., Renard, J.-B., Preissler, J., Odowd, C., 2018. Evaluation of fog and low stratus cloud microphysical properties derived from in situ sensor, cloud radar and syrsoc algorithm. *Atmosphere* 9 (5), 169.
- Duynkerke, P.G., 1999. Turbulence, radiation and fog in dutch stable boundary layers. *Bound.-Layer Meteorol.* 90 (3), 447–477.
- Duynkerke, P.G., Hignett, P., 1993. Simulation of diurnal variation in a stratocumulus-capped marine boundary layer during fire. *Mon. Weather Rev.* 121 (12), 3291–3300.
- Fabbian, D., de Dear, R., Lelyst, S., 2007. Application of artificial neural network forecasts to predict fog at Canberra international airport. *Weather Forecast.* 22 (2), 372–381.
- Fernández-González, S., Bolgiani, P., Fernández-Villares, J., González, P., Garca-Gil, A., Suárez, J.C., Merino, A., 2019. Forecasting of poor visibility episodes in the vicinity of Tenerife norte airport. *Atmos. Res.* 223, 49–59.
- Fu, G., Li, P., Crompton, J.G., Guo, S., Gao, S., Zhang, S., 2010. An observational and modeling study of a sea fog event over the yellow sea on 1 august 2003. *Meteorol. Atmos. Phys.* 107 (3–4), 149–159.
- Funk, J., 1962. Radiative flux divergence in radiation fog. *Q. J. R. Meteor. Soc.* 88 (377), 233–249.
- Goodman, J., 1977. The microstructure of California coastal fog and stratus. *J. Appl. Meteorol.* 16 (10), 1056–1067.
- Guijo-Rubio, D., Gutiérrez, P., Casanova-Mateo, C., Sanz-Justo, J., Salcedo-Sanz, S., Hervás-Martínez, C., 2018. Prediction of low-visibility events due to fog using ordinal classification. *Atmos. Res.* 214, 64–73.
- Gultepe, I., Tardif, R., Michaelides, S., Cermak, J., Bott, A., Bendix, J., Müller, M.D., Pagowski, M., Hansen, B., Ellrod, G., et al., 2007. Fog research: a review of past achievements and future perspectives. *Pure Appl. Geophys.* 164 (6–7), 1121–1159.
- Hang, C., Nadeau, D., Gultepe, I., Hoch, S., Román-Cascón, C., Pryor, K., Fernando, H., Creegan, E., Leo, L., Silver, Z., et al., 2016. A case study of the mechanisms modulating the evolution of valley fog. *Pure Appl. Geophys.* 173 (9), 3011–3030.
- Hu, H., Zhang, Q., Xie, B., Ying, Y., Zhang, J., Wang, X., 2014. Predictability of an advection fog event over North China. Part I: sensitivity to initial condition differences. *Mon. Weather Rev.* 142 (5), 1803–1822.
- Hyvärinen, O., Julkunen, J., Nietosvaara, V., may 2007. Climatological tools for low visibility forecasting. *Pure Appl. Geophys.* 164 (6–7), 1383–1396. <http://link.springer.com/10.1007/s00024-007-0224-5>.
- Koraćin, D., Lewis, J., Thompson, W.T., Dorman, C.E., Businger, J.A., 2001. Transition of stratus into fog along the California coast: observations and modeling. *J. Atmos. Sci.* 58 (13), 1714–1731.
- Kunkel, B.A., 1984. Parameterization of droplet terminal velocity and extinction coefficient in fog models. *J. Clim. Appl. Meteorol.* 23 (1), 34–41.
- McCabe, A., Swinbank, R., Tennant, W., Lock, A., 2016. Representing Model Error in the Met Office Convection Permitting Ensemble Prediction System.
- Mohan, M., Payra, S., apr 2009. Influence of aerosol spectrum and air pollutants on fog formation in urban environment of megacity Delhi, India. *Environ. Monit. Assess.* 151 (1–4), 265–277. <http://www.ncbi.nlm.nih.gov/pubmed/18379890>.
- Müller, M.D., Masbou, M., Bott, A., 2010. Three-dimensional fog forecasting in complex terrain. *Q. J. R. Meteorol. Soc.* 136 (653), 2189–2202.
- Oliver, D., Lewellen, W., Williamson, G., 1978. The interaction between turbulent and radiative transport in the development of fog and low-level stratus. *J. Atmos. Sci.* 35 (2), 301–316.
- Philip, A., Bergot, T., Bouteloup, Y., Bouysse, F., 2016. The impact of vertical resolution on fog forecasting in the kilometer-scale model arôme: a case study and statistics. *Weather Forecast.* 31 (5), 1655–1671.
- Price, J., Lane, S., Boutle, I., Smith, D., Bergot, T., Lac, C., Duconge, L., McGregor, J., Kerr-Munslow, A., Pickering, M., et al., 2018. Lanfex: a field and modeling study to improve our understanding and forecasting of radiation fog. *Bull. Am. Meteor. Soc.* 99 (10), 2061–2077.
- Roco, F.L., de Arellano, J.V.-G., Pedruzo-Bagazgoitia, X., 2018. Characterizing the influence of the marine stratocumulus cloud on the land fog at the Atacama Desert. *Atmos. Res.* 214, 109–120.
- Román-Cascón, C., Yagüe, C., Sastre, M., Maqueda, G., Salamanca, F., Viana, S., 2012.

- Observations and wrf simulations of fog events at the spanish northern plateau. *Adv. Sci. Res.* 8 (1), 11–18.
- Román-Cascón, C., Steeneveld, G., Yagüe, C., Sastre, M., Arrillaga, J., Maqueda, G., 2016a. Forecasting radiation fog at climatologically contrasting sites: evaluation of statistical methods and WRF. *Q. J. R. Meteor. Soc.* 142 (695), 1048–1063.
- Román-Cascón, C., Yagüe, C., Steeneveld, G.-J., Sastre, M., Arrillaga, J.A., Maqueda, G., 2016b. Estimating fog-top height through near-surface micrometeorological measurements. *Atmos. Res.* 170, 76–86.
- Shanyengana, E., Henschel, J., Seely, M., Sanderson, R., 2002. Exploring fog as a supplementary water source in Namibia. *Atmos. Res.* 64 (1–4), 251–259.
- Skamarock, W.C., Klemp, J.B., Dudhia, J., Gill, D.O., Barker, D.M., Wang, W., Powers, J.G., 2005. A Description of the Advanced Research WRF Version 2. Tech. Rep. National Center For Atmospheric Research Boulder Co, Mesoscale and Microscale.
- Steenefeld, G., Ronda, R., Holtslag, A., 2015. The challenge of forecasting the onset and development of radiation fog using mesoscale atmospheric models. *Bound.-Layer Meteorol.* 154 (2), 265–289.
- Tanaka, H., Honma, S., Nishi, M., Igarashi, T., Teramoto, S., Nishio, F., Abe, S., 1998. Acid fog and hospital visits for asthma: an epidemiological study. *Eur. Respir. J.* 11 (6), 1301–1306.
- Tardif, R., Rasmussen, R.M., aug 2007. Event-based climatology and typology of fog in the New York City region. *J. Appl. Meteorol. Climatol.* 46 (8), 1141–1168. <http://journals.ametsoc.org/doi/abs/10.1175/JAM2516.1>.
- Teixeira, J., 1999. Simulation of fog with the ECMWF prognostic cloud scheme. *Q. J. R. Meteorol. Soc.* 125 (554), 529–552.
- Terradellas, E., Ferreres, E., Soler, M., 2008. Analysis of turbulence in fog episodes. *Adv. Sci. Res.* 2, 31–34.
- Van der Velde, I., Steeneveld, G.J., Wichers Schreur, B., Holtslag, A.A.M., 2010. Modeling and forecasting the onset and duration of severe radiation fog under frost conditions. *Mon. Weather Rev.* 138 (11), 4237–4253.
- Van Schalkwyk, L., Dyson, L.L., 2013. Climatological characteristics of fog at Cape Town international airport. *Weather Forecast.* 28 (3), 631–646.
- Wilson, T.H., Fovell, R.G., 2018. Modeling the evolution and life cycle of radiative cold pools and fog. *Weather Forecast.* 33 (1), 203–220.
- Zhou, B., Ferrier, B.S., 2008. Asymptotic analysis of equilibrium in radiation fog. *J. Appl. Meteorol. Climatol.* 47 (6), 1704–1722.
- Zhou, B., Du, J., Gulpepe, I., Dimego, G., 2012. Forecast of low visibility and fog from NCEP: current status and efforts. *Pure Appl. Geophys.* 169 (5–6), 895–909.